

# Quasar photometric redshifts from incomplete data using Deep Learning

S. J. Curran\*

*School of Chemical and Physical Sciences, Victoria University of Wellington, PO Box 600, Wellington 6140, New Zealand*

Accepted —. Received —; in original form —

## ABSTRACT

Forthcoming astronomical surveys are expected to detect new sources in such large numbers that measuring their spectroscopic redshift measurements will be not be practical. Thus, there is much interest in using machine learning to yield the redshift from the photometry of each object. We are particularly interested in radio sources (quasars) detected with the *Square Kilometre Array* and have found Deep Learning, trained upon a large optically-selected sample of quasi-stellar objects, to be effective in the prediction of the redshifts in three external samples of radio-selected sources. However, the requirement of nine different magnitudes, from the near-infrared, optical and ultra-violet bands, has the effect of significantly reducing the number of sources for which redshifts can be predicted. Here we explore the possibility of using machine learning to impute the missing features. We find that for the training sample, simple imputation is sufficient, particularly replacing the missing magnitude with the maximum for that band, thus presuming that the non-detection is at the sensitivity limit. For the test samples, however, this does not perform as well as multivariate imputation, which suggests that many of the missing magnitudes are not limits, but have indeed not been observed. From extensive testing of the models, we suggest that the imputation is best restricted to two missing values per source. Where the sources overlap on the sky, in the worst case, this increases the fraction of sources for which redshifts can be estimated from 46% to 80%, with  $> 90\%$  being reached for the other samples.

**Key words:** techniques: photometric – methods: statistical – galaxies: active – galaxies: photometry – infrared: galaxies – ultraviolet: galaxies

## 1 INTRODUCTION

Given that large number of sources expected to be detected by forthcoming continuum surveys with the next generation of large telescopes (e.g. Norris et al. 2011; Ananna et al. 2017; Luken et al. 2019), there is currently much interest in using machine learning techniques to determine their redshifts from their photometry. These generally utilise the  $u - g$ ,  $g - r$ ,  $r - i$  and  $i - z$  colours as features to train and validate upon sources in the *Sloan Digital Sky Survey* (SDSS, e.g. Richards et al. 2001; Weinstein et al. 2004; Maddox et al. 2012; Han et al. 2016). The addition of other bands, specifically the near-infrared (NIR)  $W1$  and  $W2$  bands and the ultra-violet (UV)  $NUV$  and  $FUV$  bands, can greatly improve the accuracy of the predictions, reducing the scatter (see Sect. 2.1.3) between the predicted and actual redshifts to  $\sigma_{\Delta z(\text{norm})} \sim 0.1$  (Bovy et al. 2012; Brescia et al. 2013; Salvato et al. 2019; Curran et al. 2021). This is similar to the scatter reached by state-of-the-art template fitting of the SEDs (Hildebrandt et al. 2010; Beck et al. 2017, 2021 and references therein), although the sam-

ples are generally smaller ( $n \lesssim 10^3$ , cf.  $\gtrsim 10^4$ ) and often require the prior removal of outliers.

From our previous results (Curran & Moss 2019; Curran 2020), we (Curran et al. 2021) suggested that the wide range of magnitudes was required to cover the redshifting of rest-frame features, for example, the  $\lambda \sim 1 \mu\text{m}$  inflection and the  $\lambda = 1216 \text{ \AA}$  Lyman-break. This signifies a commonality between the data driven (machine learning) methods and the physically motivated (template fitting) methods of photometric redshift estimation (Salvato et al. 2019).

The requirement of a measurement in each of the nine bands has the effect of reducing the sample size. For example, of the 100 000 strong training sample only  $\approx 70\%$  have the full complement of measurements in all of the  $FUV$ ,  $NUV$ ,  $u$ ,  $g$ ,  $r$ ,  $i$ ,  $z$ ,  $W1$ ,  $W2$  bands (Curran et al. 2021). This worsens for the test data, which comprise three external samples of radio selected surveys, chosen to test the potential of using an SDSS trained model to predict the redshifts of *Square Kilometre Array* (SKA) (pathfinder) data (see Sect. 2.2). The common practice is to remove sources for which all of the photometry is not

\* Stephen.Curran@vuw.ac.nz

**Table 1.** The number of missing magnitude measurements in each of the bands of the 100 337 strong SDSS QSO sample. As expected, the numbers are larger for the non-SDSS photometry.

<i>FUV</i>	<i>NUV</i>	<i>u</i>	<i>g</i>	<i>r</i>	<i>i</i>	<i>z</i>	<i>W1</i>	<i>W2</i>
10 658	20 300	2923	1301	1230	1256	1258	4040	4156

available<sup>1</sup>, which can have the effect of dramatically reducing the sample size (e.g. up to half of one of our training sets). In this paper, we explore the possibility of using machine learning methods to mitigate the effect of missing data, reducing the number of sources for which we cannot obtain photometric redshifts.

## 2 ANALYSIS

### 2.1 The training data

#### 2.1.1 The data

For the training data we extracted the first 100 337 quasi-stellar objects (QSOs) with accurate spectroscopic redshifts ( $\delta z/z < 0.01$ ) from the SDSS Data Release 12 (DR12, Alam et al. 2015). We then matched the nearest source within 6 arc-seconds in the *NASA/IPAC Extragalactic Database* (NED), usually resulting in a single match. For these, the photometry was scraped from NED, WISE (Wright et al. 2010), the *Two Micron All Sky Survey* (2MASS, Skrutskie et al. 2006) and GALEX (Bianchi et al. 2017) databases. As per Curran (2020); Curran et al. (2021), in order to ensure a uniform magnitude measure between the SDSS and other samples, for each QSO we added the PSF flux densities associated with the AB magnitudes which fell within  $\Delta \log_{10} \nu = \pm 0.05$  of the central frequency of the band. Within each band range the fluxes were then averaged before being converted to a magnitude. This method, rather than just using the SDSS magnitudes directly, gives the option of using the SDSS data to train other samples, for which direct SDSS photometry may not be available.

Extensive testing showed that use of all *FUV*, *NUV*, *u*, *g*, *r*, *i*, *z*, *W1*, *W2* bands gave the most accurate photometric redshifts, with the addition of the WISE *W3*, *W4* photometry having little benefit, while significantly decreasing the sample size (Curran et al. 2021). However, even with the exclusion of the *W3*, *W4* bands, there were only 72 276 QSOs which had all of the required photometry (Table 1).

#### 2.1.2 Data imputation

Given that only 72% of the available training data are complete, we explored various methods for replacing (imputing) the missing data:

(i) *Univariate (single) imputation*: The most straightforward method, which replaces the missing magnitude with a single value. This can be done via:

(a) *Simple imputation*: Replacing the missing value with the mean, median or most frequently occurring value. An arbitrary constant may also be assigned.

(b) *Maximum value imputation*: The missing value is replaced by the detection limit (Carvajal et al. 2021), which we implemented by assuming that this was given by the largest value of the magnitude in question.

(c) *Hot-deck imputation*: The missing magnitudes are replaced by random values. We did this by generating a random number with a value between the minimum and maximum of that particular magnitude.

(ii) *Model-based imputation*: Each missing value is modelled using the other non-missing features of the dataset. A feature column (magnitude) is the output, with the remainder of the magnitudes acting as the inputs (Little & Rubin 1986; van Buuren & Groothuis-Oudshoorn 2011). We tested:

(a) *Multivariate (multiple) imputation*: A regression is fit for a known output and used to predict the empty values, which is then iterated for each feature until the maximum specified number of iterations is reached. We used the `IterativeImputer` function of `sklearn`<sup>2</sup>, with a maximum number of iterations set to 1000, in order to reach the early stopping criterion.

(b) *k-nearest neighbours (kNN) imputation*: For each missing value, the Euclidean distance is found for *k* nearest neighbours for which the feature has a value. The neighbour features can either be weighted uniformly or by the inverse of the Euclidean distance (Troyanskaya et al. 2001). This was implemented using `KNNImputer` function of `sklearn`, for which we found  $k \sim 10$  nearest neighbours uniform weighting to perform the best and so we tested this for imputed models which used  $k = 3, 10$  and  $20$ .

Since the aim is to predict the unavailable source redshifts, we removed the redshifts from the data before imputing, to ensure that these did not contribute to the machine learning. We summarise the results in Table 2 and in Fig. 1 we show the distributions of the unimputed<sup>3</sup> and imputed magnitudes. From the figure, we see that, as expected, the imputed non-SDSS photometry showed larger deviations from the measured magnitudes, most likely due to the larger number of missing values (Table 1). However, this only appears to be particularly severe for the *NUV* data, which have the most missing values. We also note that the maximum values in some bands may be due to outliers. Showing the top ends of the distributions in detail (Fig. 2), we see that this certainly appears to be the case for the *i* and WISE bands. We therefore apply the maximum value imputation, but limiting  $i \leq 23$  and  $W1 \leq 19$  and  $W2 \leq 19$  (*maximum truncated* in Table 2).

#### 2.1.3 Deep Learning

As described in Curran et al. (2021), the Deep Learning model, built with the `TensorFlow`<sup>4</sup> platform, outperformed both the *k-Nearest Neighbour* (kNN) and *Decision Tree Regression* algorithms, with self validation giving a regression coefficient of the least-squares linear fit between the predicted and measured redshifts of  $r = 0.94$ . As with other studies, we used the colours as features (Sect. 1), although we noted that using the raw magnitudes gave a similar performance. Since replacing missing magnitudes is

<sup>1</sup> Exceptions are Bovy et al. (2012), who use the probability distribution in the feature–redshift space of the other sources to fill in the missing values, and Carvajal et al. (2021), who assume the detection limit of that band for the missing values.

<sup>2</sup> <https://scikit-learn.org/stable/>

<sup>3</sup> We use *un-imputed* to refer to the full 100 337 sample with the missing values included and *non-imputed* for the 72 276 sources with all nine magnitudes.

<sup>4</sup> <https://www.tensorflow.org>

**Table 2.** The statistics of the un-imputed and imputed SDSS QSO data. Where the minimum and maximum are not shown where these are the same as the un-imputed data.

	Redshift	<i>FUV</i>	<i>NUV</i>	<i>u</i>	<i>g</i>	<i>r</i>	<i>i</i>	<i>z</i>	<i>W1</i>	<i>W2</i>
UN-IMPURED (missing values included)										
<i>n</i>	100 337	89 679	80 037	97 414	99 036	99 107	99 081	99 079	96 297	96 181
mean	1.483	20.81	20.57	19.76	19.39	19.14	18.98	18.91	15.16	14.21
std	0.878	0.95	1.26	1.27	0.19	0.77	0.74	0.75	0.91	0.97
min	0.0046	16.07	15.25	15.38	14.47	14.38	13.61	13.74	9.91	8.90
max	6.999	24.92	25.53	31.85	29.32	22.62	27.17	24.26	27.84	27.70
UNIVARIATE (mean), <i>n</i> = 100 337										
mean	—	20.81	20.57	19.76	19.39	19.14	18.98	18.91	15.16	14.21
std	—	0.90	1.13	1.25	0.89	0.76	0.74	0.75	0.89	0.95
UNIVARIATE (median), <i>n</i> = 100 337										
mean	—	20.81	20.55	19.75	19.39	19.14	18.98	18.91	15.16	14.21
std	—	0.90	1.13	1.25	0.89	0.76	0.74	0.75	0.89	0.95
UNIVARIATE (most frequent), <i>n</i> = 100 337										
mean	—	20.87	20.51	19.73	19.38	19.14	18.98	18.91	15.16	14.20
std	—	0.91	1.14	1.26	0.89	0.77	0.74	0.74	0.89	0.95
UNIVARIATE (maximum), <i>n</i> = 100 337										
mean	—	21.25	21.58	20.11	19.52	19.18	19.09	18.97	15.67	14.77
std	—	1.55	2.29	2.39	1.43	0.855	1.17	0.953	2.65	2.85
UNIVARIATE (maximum truncated), <i>n</i> = 100 337										
mean	—	21.25	21.58	20.11	19.52	19.18	19.03	18.97	15.29	14.35
std	—	1.55	2.29	2.39	1.43	0.86	0.83	0.95	1.09	1.16
max	—	24.92	25.53	31.85	29.32	22.62	23.0	24.26	19.0	19.0
UNIVARIATE (random), <i>n</i> = 100 337										
mean	—	20.81	20.57	19.76	19.39	19.14	18.98	18.91	15.16	14.21
std	—	0.95	1.26	1.27	0.90	0.77	0.74	0.75	0.91	0.97
MULTIVARIATE, <i>n</i> = 100 337										
mean	—	20.83	20.80	19.82	19.40	19.14	18.99	18.91	15.18	14.23
std	—	0.94	1.42	1.34	0.90	0.77	0.74	0.75	15.18	14.23
min	—	16.07	10.21	15.38	14.47	14.38	13.60	13.74	9.91	8.90
max	—	27.41	33.22	36.82	29.32	22.62	27.17	26.22	27.84	27.70
kNN ( <i>k</i> = 3), <i>n</i> = 100 337										
mean	—	20.83	20.59	19.84	19.40	19.14	18.99	18.91	15.17	14.23
std	—	0.94	1.21	1.37	0.90	0.77	0.74	0.75	0.90	0.97
kNN ( <i>k</i> = 10), <i>n</i> = 100 337										
mean	—	20.82	20.62	19.84	19.40	19.14	18.99	18.91	15.17	14.23
std	—	0.93	1.19	1.37	0.90	0.77	0.74	0.75	0.90	0.97
kNN ( <i>k</i> = 20), <i>n</i> = 100 337										
mean	—	20.82	20.65	19.84	19.40	19.14	18.98	18.91	15.17	14.23
std	—	0.92	1.10	1.36	0.90	0.77	0.74	0.75	0.90	0.97

more straightforward than colours, we use the magnitudes as features here.

Upon imputing the data, we trained the model on a random 80% portion, using the same Deep Learning model as previously – two *Rectified Linear Unit* (ReLU) function layers and one *hyperbolic tangent* (tanh) layer comprising 200 neurons each. We then validated the model on the remaining 20% of the data, comparing

the photometric (predicted) redshifts with the spectroscopic (measured) redshifts, which had been returned to the imputed dataset. In order to account for the small differences in the results inherent between each trial, we then reshuffled the data and repeated the process 99 times. We summarise the results in Table 3, using statistics calculated for the difference between the photometric and spectroscopic redshifts,  $\Delta z \equiv z_{\text{spec}} - z_{\text{phot}}$ , and its normalized

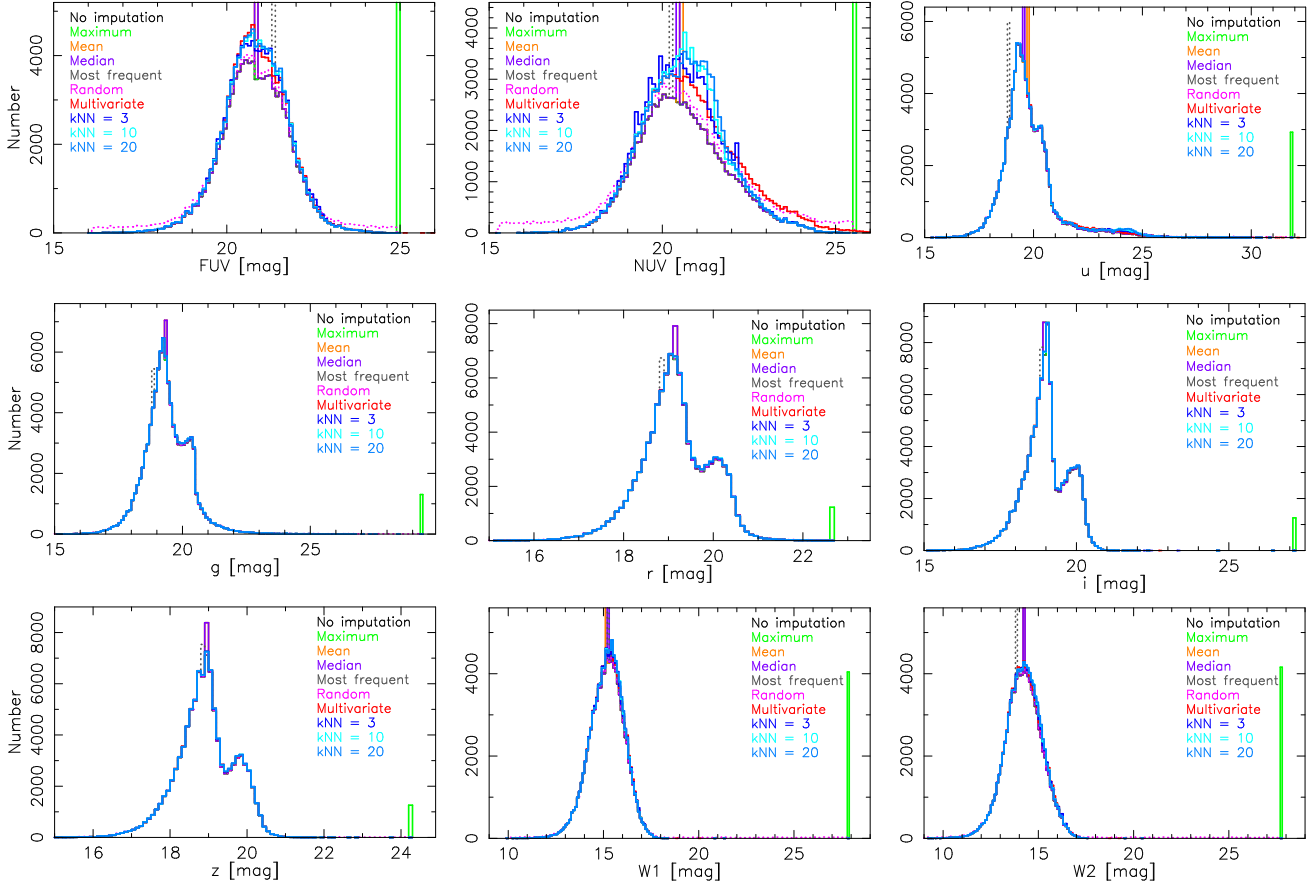


**Figure 1.** The distribution of each of the magnitudes for various imputation methods. Note that the un-imputed, maximum, mean, median and most frequent distributions are coincident apart from the spikes introduced by these methods.

**Table 3.** The mean results of the SDSS validation (20 067 sources) for the various imputation methods over randomized 100 trials, quoted with  $\pm 1\sigma$ . For the non-imputed data there are 14 253 validation sources.

Imputation	$r$	Un-normalised			Normalised		
		$\mu_{\Delta z}$	$\sigma_{\Delta z}$	$\sigma_{\text{MAD}}$	$\mu_{\Delta z(\text{norm})}$	$\sigma_{\Delta z(\text{norm})}$	$\sigma_{\text{NMAD}}$
None	$0.934 \pm 0.002$	$0.003 \pm 0.032$	$0.234 \pm 0.003$	$0.105 \pm 0.012$	$-0.008 \pm 0.015$	$0.115 \pm 0.005$	$0.048 \pm 0.006$
Univariate							
Mean	$0.918 \pm 0.002$	$0.003 \pm 0.034$	$0.351 \pm 0.004$	$0.132 \pm 0.012$	$-0.017 \pm 0.017$	$0.162 \pm 0.006$	$0.055 \pm 0.005$
Median	$0.919 \pm 0.002$	$0.002 \pm 0.032$	$0.349 \pm 0.004$	$0.129 \pm 0.011$	$-0.016 \pm 0.015$	$0.162 \pm 0.006$	$0.054 \pm 0.005$
Most	$0.918 \pm 0.002$	$0.002 \pm 0.032$	$0.352 \pm 0.004$	$0.130 \pm 0.010$	$-0.016 \pm 0.015$	$0.166 \pm 0.006$	$0.055 \pm 0.004$
Max	$0.927 \pm 0.002$	$0.004 \pm 0.035$	$0.332 \pm 0.005$	$0.124 \pm 0.015$	$-0.014 \pm 0.017$	$0.155 \pm 0.009$	$0.051 \pm 0.007$
Max trun.	$0.933 \pm 0.003$	$0.003 \pm 0.037$	$0.315 \pm 0.007$	$0.127 \pm 0.017$	$-0.014 \pm 0.016$	$0.154 \pm 0.009$	$0.052 \pm 0.005$
Random	$0.909 \pm 0.002$	$0.006 \pm 0.032$	$0.369 \pm 0.005$	$0.134 \pm 0.011$	$-0.166 \pm 0.015$	$0.175 \pm 0.007$	$0.056 \pm 0.004$
Multivariate	$0.916 \pm 0.002$	$0.000 \pm 0.032$	$0.355 \pm 0.005$	$0.130 \pm 0.012$	$-0.018 \pm 0.015$	$0.167 \pm 0.008$	$0.055 \pm 0.005$
kNN							
$k = 3$	$0.903 \pm 0.002$	$-0.004 \pm 0.030$	$0.380 \pm 0.004$	$0.138 \pm 0.009$	$-0.022 \pm 0.013$	$0.180 \pm 0.007$	$0.058 \pm 0.004$
$k = 10$	$0.909 \pm 0.002$	$-0.003 \pm 0.029$	$0.369 \pm 0.004$	$0.132 \pm 0.011$	$-0.021 \pm 0.013$	$0.175 \pm 0.006$	$0.056 \pm 0.005$
$k = 20$	$0.912 \pm 0.002$	$0.001 \pm 0.026$	$0.364 \pm 0.004$	$0.129 \pm 0.010$	$-0.019 \pm 0.012$	$0.172 \pm 0.007$	$0.054 \pm 0.004$

counterpart,  $\Delta z(\text{norm}) \equiv \frac{z_{\text{spec}} - z_{\text{phot}}}{z_{\text{spec}} + 1}$ . Specifically, the mean difference between the photometric and spectroscopic redshifts,

$$\mu_{\Delta z} \equiv \frac{1}{N} \sum_{i=1}^N \Delta z_i,$$

the standard deviation,

$$\sigma_{\Delta z} \equiv \sqrt{\frac{1}{N} \sum_{i=1}^N \Delta z_i^2},$$

and the median absolute deviation (MAD),

$$\sigma_{\text{MAD}} \equiv 1.48 \times \text{median} |z_{\text{spec}} - z_{\text{phot}}|.$$

We confirm that using the magnitudes directly performs as

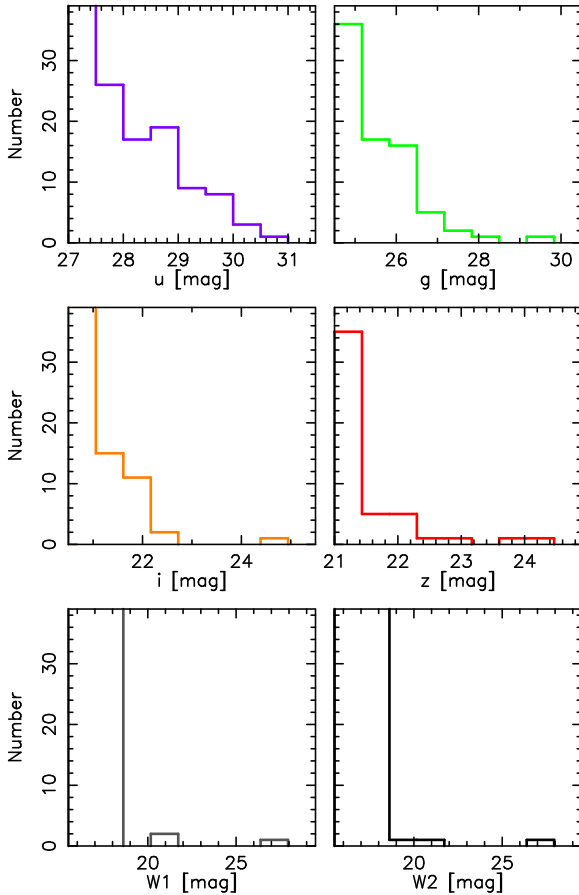


**Figure 2.** The upper extremes of the magnitudes of the un-imputed data with suspected outliers.

well as the  $FUV - NUV$ ,  $NUV - u$ ,  $u - g$ ,  $g - r$ ,  $r - i$ ,  $i - z$ ,  $z - W1$  &  $W1 - W2$  colours, where the regression coefficient was  $r \approx 0.94$ ,  $\sigma_{\Delta z} \approx 0.235$  and  $\sigma_{\text{MAD}} \approx 0.092$  (Curran et al. 2021).<sup>5</sup> We also see that the best performing imputation method is the *maximum truncated*, with  $\bar{r} = 0.933$ ,  $\overline{\sigma_{\Delta z}} = 0.315$  and  $\overline{\sigma_{\text{MAD}}} = 0.127$ . This uses a similar method as Carvajal et al. (2021), who assume the detection limit for each missing value. According to their chosen metric, the *normalised median absolute deviation* (NMAD),

$$\sigma_{\text{NMAD}} \equiv 1.48 \times \text{median} \left| \frac{z_{\text{spec}} - z_{\text{phot}}}{z_{\text{spec}} + 1} \right|,$$

our model performs slightly better than theirs (all have  $\sigma_{\text{NMAD}} > 0.06$ , cf. our 0.052). As previously noted (Curran et al. 2021), Deep Learning gives better results across all metrics, including  $\sigma_{\text{NMAD}}$ , than standard machine learning algorithms (namely,  $k$ -Nearest Neighbour and Decision Tree Regression).

## 2.2 The test data

### 2.2.1 The data

As stated above, our goal is to develop photometric redshift models for radio sources detected with the SKA and its pathfinders. As described in Curran & Moss (2019), finding large catalogues of radio

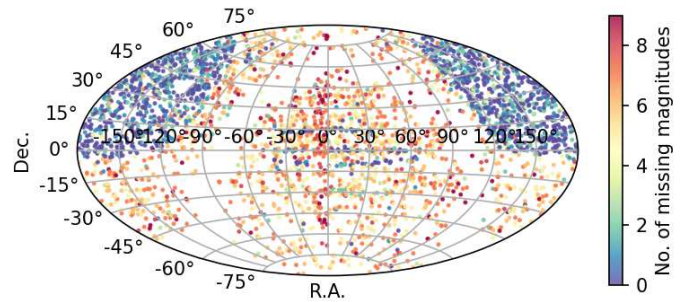


**Figure 3.** The sky distribution of the OCARS sources, colour coded by the number of missing magnitudes per source.

sources with spectroscopic redshifts is a challenge and just three sizable databases were found:

(i) The *Faint Images of the Radio Sky at Twenty-Centimeters* (FIRST, Becker et al. 1995; White et al. 1997), which has 18 273 sources with redshifts from the SDSS DR14 QSOs (Pâris et al. 2018). Of these, 9016 are classed as QSOs in NED.

(ii) The *Large Area Radio Galaxy Evolution Spectroscopic Survey* (LARGESS). Of the 10 685 sources with optical redshifts (Ching et al. 2017)<sup>6</sup>, 1608 are classified as quasars in NED. Although termed “radio-loud”, these have a similar distribution of radio fluxes as the SDSS sample (Curran et al. 2021) and so we refer to these as QSOs.

(iii) The *Optical Characteristics of Astrometric Radio Sources* (OCARS) catalogue of *Very Long Baseline Interferometry* (VLBI) astrometry sources (Ma et al. 2009; Malkin 2018). Of the 3663 sources, 2404 are classified as quasars, but given that these are very strong radio calibration sources we assume that all of the non-galaxies are active galactic nuclei (AGN), giving a sample size of 3033.

Again, the requirement of measured magnitudes in all nine bands has the effect of cutting the samples, leaving 65% of the LARGESS sample, 57% of the FIRST sample and just 21% of the OCARS sample. The large fraction of missing data in the latter is due a mismatch between this and the SDSS’s sky coverage, which is restricted to the northern sky (Fig.3). In Fig. 4, we show distribution of the number of missing magnitudes per source, from which we see that OCARS is most likely to have 5–7 magnitudes missing, in addition to a large proportion of sources having no magnitude measurements at all.

### 2.2.2 Data imputation and machine learning

We impute the missing values using the same methods as for the SDSS data (Sect. 2.1.2). The only method we exclude is the *maximum truncated*, since the maximum values for the test data do not indicate the presence of extreme outliers (Table 4). Following the imputation and upon returning the spectroscopic redshifts to the data, we train the model using the non-imputed SDSS photometry (72 276 QSOs), which we then validate on each test sample,

<sup>5</sup> These are given as approximations since they are from a single run of the model.

<sup>6</sup> Those with redshift reliability flag  $q \geq 3$ , where  $q = 3$  designates “a reasonably confident redshift”, and the maximum  $q = 5$  designates an “extremely reliable redshift from a good-quality spectrum”.

**Table 4.** The statistics for the test samples.  $N$  is the number of sources for which the magnitude is available, followed by the percentage of the total. This is followed by the minimum, maximum, mean, median and most frequently measured value of the magnitude.

Mag.	$N$	%	min	max	mean	median	most
FIRST, $n = 9016$							
<i>FUV</i>	6912	77	16.07	25.03	20.78	20.85	21.38
<i>NUV</i>	6699	74	14.83	25.40	20.57	20.52	21.43
<i>u</i>	8457	94	14.22	28.45	19.76	19.65	18.88
<i>g</i>	8672	95	14.49	26.34	19.30	19.32	18.87
<i>r</i>	8587	95	14.38	22.18	19.02	19.07	18.87
<i>i</i>	8564	95	14.45	22.06	18.85	18.92	18.85
<i>z</i>	8563	95	14.35	22.55	18.75	18.83	18.81
<i>W1</i>	8563	95	9.84	18.34	14.96	15.05	15.84
<i>W2</i>	8552	95	8.90	17.97	14.05	14.14	14.81
LARGESS, $n = 1608$							
<i>FUV</i>	1265	79	16.02	24.40	21.23	21.23	20.27
<i>NUV</i>	1373	85	15.79	24.92	20.96	21.02	19.73
<i>u</i>	1549	96	15.65	30.36	20.13	20.10	20.97
<i>g</i>	1583	98	14.27	24.16	19.67	19.72	20.38
<i>r</i>	1582	98	14.09	22.21	19.34	19.43	18.74
<i>i</i>	1579	98	13.61	21.49	19.14	19.26	18.85
<i>z</i>	1579	98	13.61	23.30	19.01	19.13	18.81
<i>W1</i>	1468	91	10.12	17.77	15.02	15.16	14.61
<i>W2</i>	1466	91	8.89	17.04	14.17	14.32	15.15
OCARS, $n = 3033$							
<i>FUV</i>	1434	47	13.51	24.90	20.22	20.31	20.82
<i>NUV</i>	2035	67	13.56	24.66	20.01	20.01	21.15
<i>u</i>	1170	39	12.78	27.47	19.30	19.18	18.26
<i>g</i>	1255	41	12.45	26.34	18.86	18.78	18.74
<i>r</i>	1374	45	12.77	26.28	18.57	18.55	18.75
<i>i</i>	1264	42	11.67	24.09	18.45	18.48	18.70
<i>z</i>	1205	40	12.69	23.13	18.30	18.34	18.61
<i>W1</i>	2562	84	7.26	17.56	14.20	14.33	13.77
<i>W2</i>	2562	84	6.26	17.23	13.30	13.39	13.54

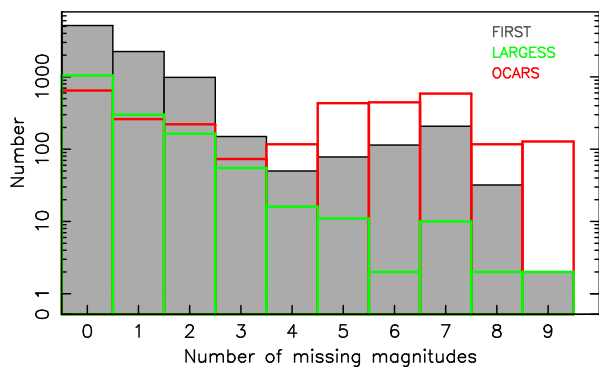


**Figure 4.** Histograms of the total number of missing magnitudes per source for the three test samples.

again comparing the predicted with the measured redshifts (Table 5). We see that replacing the missing magnitudes via machine learning methods (multivariate and kNN imputation) significantly outperform the simple (univariate and random) methods, although replacement with the maximum value remains the best of these. The effectiveness of applying the maximum value to the SDSS data likely stems from many of the missing values actually being due

to sensitivity limits, whereas for data drawn independently of the SDSS (i.e. OCARS), a larger fraction of the missing data are expected to be due to non-measurements.

In order to place the OCARS data on a more equal par with the other test samples, we now consider only the OCARS sources with at least one SDSS magnitude, thus being more likely to having overlapping coordinates (Table 6). Applying the Deep Learning to this data (Table 7), we see again that the multivariate method is the best, although in general the results are inferior to those of the FIRST and LARGESS samples. However, even with the requirement of at least one SDSS magnitude, only 46% of the OCARS sources have the full magnitude complement.

## 3 DISCUSSION

### 3.1 Results

#### 3.1.1 General

Training and validating on the 100 337 strong SDSS sample, for which 28% of sources have at least one missing magnitude, we find all of the imputation methods to be effective, with the randomly selected 20 067 validation sources giving regression coefficients of  $r \gtrsim 0.9$  between the predicted and measured redshifts. These compare favourably with  $r = 0.91 - 0.94$  obtained when using the source colours as features. The best performing method was replacement by the maximum for the band in question ( $r = 0.93$ ), similar to the imputation method of Carvajal et al. (2021), who assume that each missing value is at the detection limit.

Training on the 72 276 QSOs which have all nine magnitudes and testing on the three other, radio-selected, catalogues, we find multivariate imputation to perform the best, although we only achieve  $\bar{r} = 0.60$  for the OCARS sample. However, only 47% of the sources have an SDSS magnitude, due to the full sky distribution of OCARS, and considering only these increases the regression coefficient to  $\bar{r} = 0.74$ . This is still low, which we believe is due to only 46% of this 47% having all of the nine magnitudes.

#### 3.1.2 OCARS

As discussed above, the machine learning performs poorest when applied to the OCARS data. This may not be surprising since, unlike the LARGESS and FIRST data (Ching et al. 2017; Pâris et al. 2018), OCARS is compiled independently of the SDSS. Also, the mean radio flux density for the OCARS sources is an order of magnitude higher than the others. These, unlike OCARS, appear to be truncated at the lower flux densities ( $S_{\text{radio}} \lesssim 1$  mJy), suggesting a flux limitation (Curran et al. 2021). Hence, both the LARGESS and SDSS data may be more representative of future continuum radio surveys, which are expected to be sensitive to flux densities of  $S_{\text{radio}} \sim 0.1$  mJy (e.g. Norris et al. 2011). We should, however, not yet rule out using the SDSS to train the NIR-optical-UV photometry of radio-loud sources.

In Fig. 5, we show how the imputation affects the Deep Learning results for the OCARS quasars as more missing magnitudes are replaced. For all cases, we see that the redshift accuracy is relatively poor at  $z \lesssim 0.5$ , which was also noted for the non-imputed data. We (Curran et al. 2021) suggested that this was due to limitations in the FUV magnitudes, which are required to accurately trace the Lyman break at  $z \sim 0$  and in Fig. 6 we see that the FUV has the largest fraction of missing values at low redshift. We also see that

**Table 5.** The mean results for the various imputation methods over 10 trials, quoted with  $\pm 1\sigma$ .

Imputation	$n$	$r$	Un-normalised			Normalised		
			$\mu_{\Delta z}$	$\sigma_{\Delta z}$	$\sigma_{\text{MAD}}$	$\mu_{\Delta z(\text{norm})}$	$\sigma_{\Delta z(\text{norm})}$	$\sigma_{\text{NMAD}}$
FIRST								
None	5147	$0.949 \pm 0.004$	$0.031 \pm 0.019$	$0.206 \pm 0.006$	$0.116 \pm 0.005$	$0.008 \pm 0.009$	$0.094 \pm 0.002$	$0.052 \pm 0.002$
Univariate								
Mean	9016	$0.752 \pm 0.014$	$0.109 \pm 0.052$	$0.554 \pm 0.005$	$0.176 \pm 0.014$	$0.014 \pm 0.024$	$0.202 \pm 0.009$	$0.075 \pm 0.007$
Median	9016	$0.740 \pm 0.033$	$0.121 \pm 0.039$	$0.564 \pm 0.032$	$0.169 \pm 0.012$	$0.018 \pm 0.015$	$0.206 \pm 0.005$	$0.072 \pm 0.005$
Most	9016	$0.683 \pm 0.048$	$0.180 \pm 0.054$	$0.611 \pm 0.038$	$0.184 \pm 0.010$	$0.035 \pm 0.021$	$0.208 \pm 0.011$	$0.081 \pm 0.005$
Max	9016	$0.771 \pm 0.012$	$-0.141 \pm 0.026$	$0.597 \pm 0.028$	$0.172 \pm 0.009$	$-0.078 \pm 0.009$	$0.299 \pm 0.018$	$0.070 \pm 0.004$
Random	9016	$0.680 \pm 0.030$	$0.026 \pm 0.072$	$0.648 \pm 0.025$	$0.191 \pm 0.009$	$-0.024 \pm 0.027$	$0.276 \pm 0.108$	$0.081 \pm 0.005$
Multivariate	9016	$0.904 \pm 0.005$	$0.020 \pm 0.025$	$0.359 \pm 0.010$	$0.146 \pm 0.009$	$-0.004 \pm 0.011$	$0.155 \pm 0.006$	$0.060 \pm 0.001$
kNN								
$k = 3$	9016	$0.839 \pm 0.017$	$0.069 \pm 0.051$	$0.046 \pm 0.021$	$0.159 \pm 0.014$	$0.009 \pm 0.021$	$0.170 \pm 0.003$	$0.066 \pm 0.006$
$k = 10$	9016	$0.872 \pm 0.012$	$0.054 \pm 0.027$	$0.409 \pm 0.019$	$0.149 \pm 0.007$	$0.006 \pm 0.004$	$0.160 \pm 0.005$	$0.063 \pm 0.001$
$k = 20$	9016	$0.890 \pm 0.007$	$0.022 \pm 0.028$	$0.382 \pm 0.011$	$0.144 \pm 0.006$	$-0.006 \pm 0.013$	$0.155 \pm 0.005$	$0.060 \pm 0.002$
LARGESS								
None	1046	$0.913 \pm 0.005$	$0.042 \pm 0.022$	$0.292 \pm 0.008$	$0.128 \pm 0.005$	$0.008 \pm 0.012$	$0.116 \pm 0.009$	$0.061 \pm 0.002$
Univariate								
Mean	1608	$0.720 \pm 0.020$	$0.080 \pm 0.053$	$0.610 \pm 0.022$	$0.172 \pm 0.011$	$-0.005 \pm 0.023$	$0.271 \pm 0.031$	$0.077 \pm 0.006$
Median	1608	$0.723 \pm 0.012$	$0.075 \pm 0.033$	$0.605 \pm 0.012$	$0.175 \pm 0.020$	$-0.008 \pm 0.018$	$0.271 \pm 0.021$	$0.079 \pm 0.010$
Most	1608	$0.641 \pm 0.024$	$0.105 \pm 0.049$	$0.683 \pm 0.025$	$0.196 \pm 0.020$	$-0.005 \pm 0.022$	$0.305 \pm 0.025$	$0.088 \pm 0.009$
Max	1608	$0.809 \pm 0.013$	$-0.036 \pm 0.026$	$0.531 \pm 0.027$	$0.171 \pm 0.009$	$-0.041 \pm 0.013$	$0.297 \pm 0.021$	$0.074 \pm 0.003$
Random	1608	$0.621 \pm 0.025$	$0.024 \pm 0.046$	$0.742 \pm 0.040$	$0.190 \pm 0.008$	$-0.034 \pm 0.019$	$0.361 \pm 0.029$	$0.085 \pm 0.005$
Multivariate	1608	$0.829 \pm 0.012$	$0.028 \pm 0.025$	$0.488 \pm 0.017$	$0.157 \pm 0.006$	$-0.013 \pm 0.011$	$0.224 \pm 0.021$	$0.068 \pm 0.002$
kNN								
$k = 3$	1608	$0.814 \pm 0.010$	$0.023 \pm 0.024$	$0.511 \pm 0.018$	$0.162 \pm 0.007$	$-0.017 \pm 0.012$	$0.249 \pm 0.019$	$0.071 \pm 0.003$
$k = 10$	1608	$0.816 \pm 0.016$	$0.031 \pm 0.028$	$0.506 \pm 0.026$	$0.013 \pm 0.007$	$-0.013 \pm 0.015$	$0.242 \pm 0.027$	$0.070 \pm 0.003$
$k = 20$	1608	$0.811 \pm 0.010$	$0.044 \pm 0.048$	$0.513 \pm 0.022$	$0.161 \pm 0.007$	$-0.009 \pm 0.021$	$0.238 \pm 0.034$	$0.071 \pm 0.003$
OCARS								
None	649	$0.867 \pm 0.010$	$0.048 \pm 0.043$	$0.339 \pm 0.003$	$0.144 \pm 0.013$	$0.008 \pm 0.025$	$0.159 \pm 0.014$	$0.066 \pm 0.007$
Univariate								
Mean	3033	$0.482 \pm 0.020$	$0.181 \pm 0.015$	$0.823 \pm 0.012$	$0.476 \pm 0.017$	$0.015 \pm 0.015$	$0.337 \pm 0.009$	$0.218 \pm 0.009$
Median	3033	$0.483 \pm 0.011$	$0.114 \pm 0.055$	$0.821 \pm 0.013$	$0.478 \pm 0.016$	$-0.017 \pm 0.026$	$0.350 \pm 0.011$	$0.217 \pm 0.008$
Most	3033	$0.421 \pm 0.018$	$0.190 \pm 0.047$	$0.807 \pm 0.011$	$0.518 \pm 0.022$	$-0.002 \pm 0.008$	$0.224 \pm 0.08$	$0.238 \pm 0.006$
Max	3033	$0.346 \pm 0.048$	$0.281 \pm 0.165$	$0.943 \pm 0.049$	$0.638 \pm 0.060$	$0.041 \pm 0.073$	$0.411 \pm 0.032$	$0.313 \pm 0.039$
Random	3033	$0.282 \pm 0.014$	$0.070 \pm 0.100$	$1.043 \pm 0.040$	$0.720 \pm 0.039$	$-0.055 \pm 0.046$	$0.478 \pm 0.024$	$0.321 \pm 0.018$
Multivariate	3033	$0.597 \pm 0.011$	$0.240 \pm 0.050$	$0.722 \pm 0.009$	$0.379 \pm 0.013$	$0.050 \pm 0.024$	$0.284 \pm 0.008$	$0.183 \pm 0.007$
kNN								
$k = 3$	3033	$0.506 \pm 0.008$	$0.238 \pm 0.040$	$0.813 \pm 0.011$	$0.466 \pm 0.011$	$0.043 \pm 0.018$	$0.326 \pm 0.013$	$0.221 \pm 0.004$
$k = 10$	3033	$0.513 \pm 0.017$	$0.314 \pm 0.032$	$0.785 \pm 0.010$	$0.438 \pm 0.018$	$0.078 \pm 0.015$	$0.295 \pm 0.002$	$0.215 \pm 0.009$
$k = 20$	3033	$0.540 \pm 0.026$	$0.310 \pm 0.028$	$0.767 \pm 0.015$	$0.444 \pm 0.023$	$0.077 \pm 0.017$	$0.290 \pm 0.008$	$0.212 \pm 0.011$

the fraction of missing values increases across all bands with increasing redshift, thus requiring a larger degree of imputation. This is evident in Fig. 5 with higher redshifts being attainable with the imputation of more missing values, although at a cost in accuracy.

Imputing all of the missing magnitudes we would retain the whole training sample. Knowing that the higher redshifts are less accurate, we could, in principle, assign a confidence in the prediction dependent upon the redshift. But since in practice the redshifts will be unknown a priori, we would require a means of approximately estimating these. Both Curran & Moss (2019) and Li et al. (2021) use a two step approach, first splitting the sources into low and high redshift samples. Specifically, Curran & Moss used the correlation between the  $W2$  magnitude and redshift (Glowacki et al. 2017), to obtain an approximate redshift, before proceeding with a more detailed determination. However, as seen

from Fig. 7, this has a large uncertainty and any  $W2$ -redshift relation will already be incorporated into the Deep Learning.

### 3.2 Imputation limits

In Fig. 8, we show the degradation in the performance as more missing values are replaced for the three test datasets. While these are examples of the overall performance, in order to obtain real insight into how far it is sensible to impute, we require the mean Deep Learning metrics for each number of missing magnitudes per source: For the FIRST sample (Fig. 9, top), we see that most sources have less than three missing magnitudes and if we limit the imputation to this number, the predicted redshifts retain a relatively high quality.

For the LARGESS sample (Fig. 9, middle) we see a similar situation, although the decrease in the number of sources as the

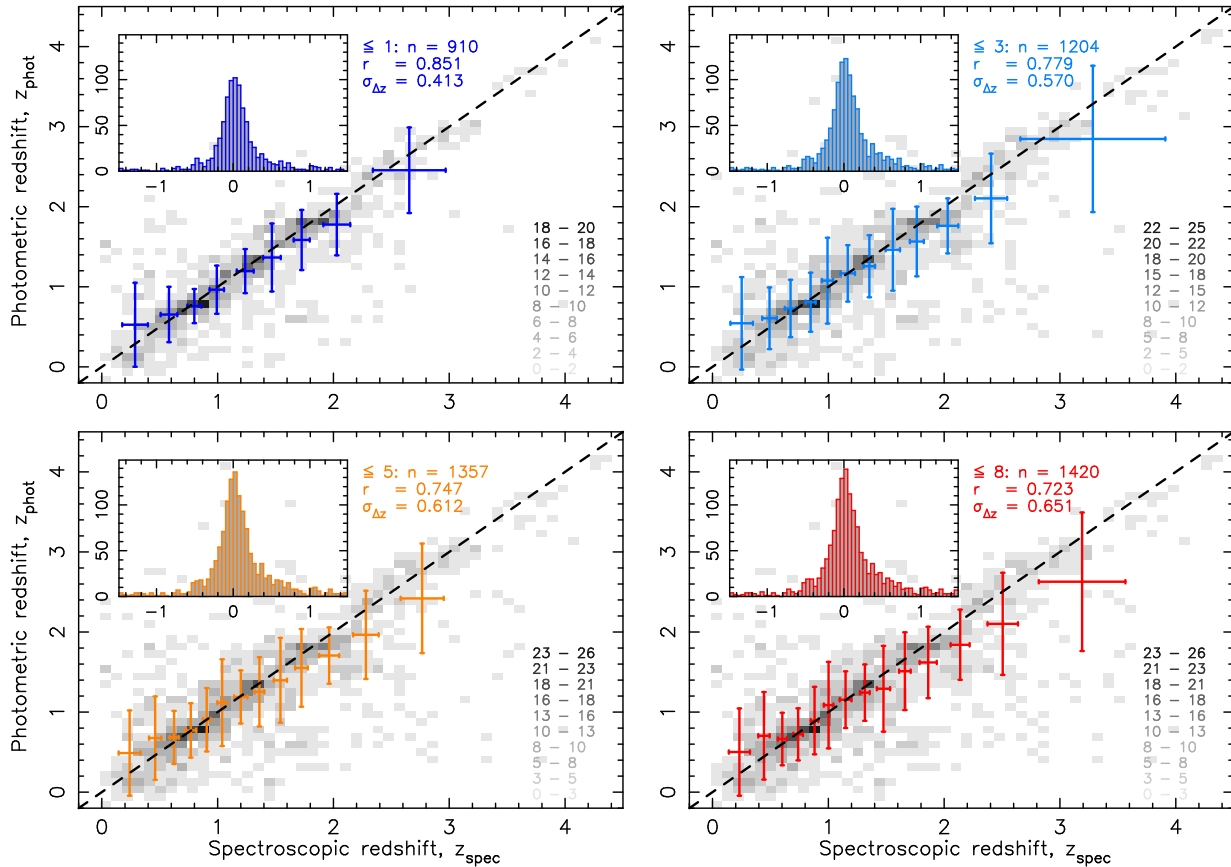


**Figure 5.** The photometric versus the spectroscopic redshift for different numbers of imputed magnitudes (up to 1,3,5 & 8) per source for the OCARS sources with at least one SDSS match. The grey-scale shows the source distribution with the key on the bottom right showing the number within each pixel. The binning is for an equal number of sources in each bin (100) with the error bars showing  $\pm 1\sigma$ . The broken line shows  $z_{\text{phot}} = z_{\text{spec}}$  and the inset the distribution of  $\Delta z$ . Note that this is from a single Deep Learning trial and so the values should be considered approximate only, e.g.  $r = 0.723$  for full imputation, cf  $\bar{r} = 0.737$  (Table 7).

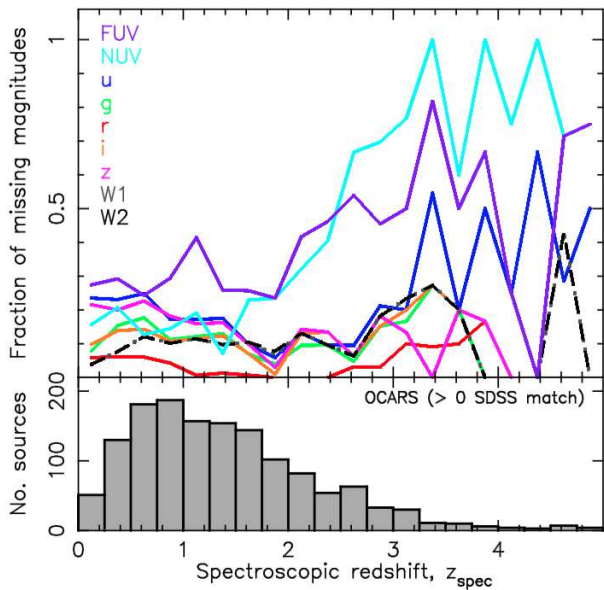


**Figure 6.** The fraction of missing magnitudes in each band (top) and the number of sources (bottom) for the OCARS sources with at least one SDSS match.

**Table 6.** The statistics for the OCARS quasars with at least one SDSS magnitude (1420 sources), cf. Table 4.

Mag.	$n$	%	min	max	mean	median	most
<i>FUV</i>	946	67	13.51	24.90	20.09	20.15	20.39
<i>NUV</i>	1059	75	13.57	24.66	19.83	19.71	20.50
<i>u</i>	1170	82	12.78	27.47	19.30	19.18	18.26
<i>g</i>	1255	88	12.45	26.34	18.86	18.78	18.74
<i>r</i>	1374	97	12.77	26.28	18.57	18.55	18.75
<i>i</i>	1264	89	11.67	24.09	18.45	18.48	18.70
<i>z</i>	1205	85	12.69	23.13	18.30	18.34	18.61
<i>W1</i>	1269	89	8.31	17.56	14.19	14.33	14.65
<i>W2</i>	1268	89	7.05	16.55	13.25	13.34	14.78

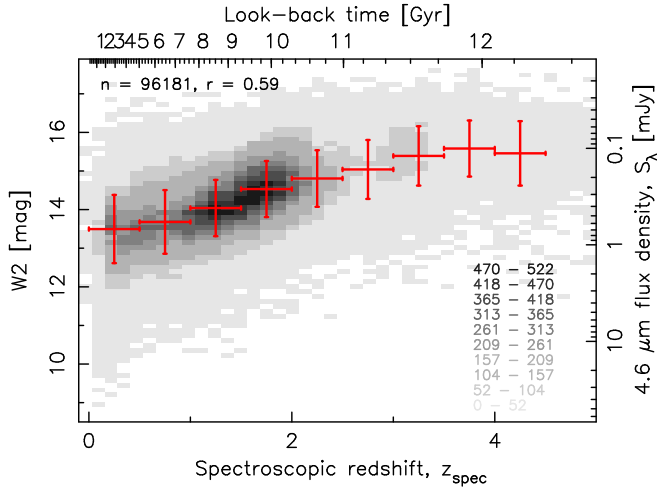
number of missing values increases is more gradual. Nevertheless, since we start with a smaller sample, there are only 55 sources with three missing magnitudes, falling to 16 with four. Again, the best results cluster at less than three imputed magnitudes per source, with the error bars indicating considerably less scatter between the Deep Learning runs. Note that there are only two sources with six imputed magnitudes, resulting in the large errors, e.g.  $\bar{r} = 0.4 \pm 0.9$ .

For the OCARS sample (Fig. 9, bottom), again we see a large drop in performance when more than two magnitudes are imputed.



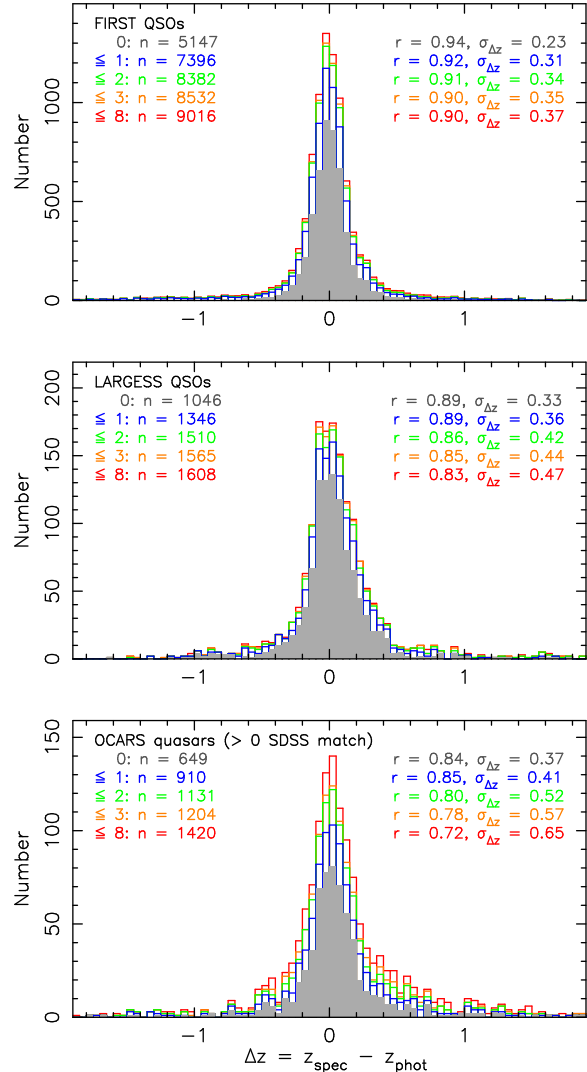
**Table 7.** As Table 5, but for the OCARS sources with at least one SDSS magnitude measurement.

Imputation	$n$	$r$	Un-normalised			Normalised		
			$\mu_{\Delta z}$	$\sigma_{\Delta z}$	$\sigma_{\text{MAD}}$	$\mu_{\Delta z(\text{norm})}$	$\sigma_{\Delta z(\text{norm})}$	$\sigma_{\text{NMAD}}$
OCARS ( $\geq 0$ SDSS match)								
Univariate								
Mean	1420	$0.546 \pm 0.023$	$0.232 \pm 0.060$	$0.804 \pm 0.014$	$0.263 \pm 0.023$	$0.039 \pm 0.028$	$0.310 \pm 0.014$	$0.125 \pm 0.010$
Median	1420	$0.544 \pm 0.022$	$0.218 \pm 0.056$	$0.801 \pm 0.026$	$0.267 \pm 0.011$	$0.032 \pm 0.026$	$0.314 \pm 0.023$	$0.128 \pm 0.006$
Most	1420	$0.529 \pm 0.026$	$0.191 \pm 0.075$	$0.816 \pm 0.025$	$0.320 \pm 0.015$	$0.017 \pm 0.033$	$0.317 \pm 0.007$	$0.153 \pm 0.008$
Max	1420	$0.574 \pm 0.030$	$-0.032 \pm 0.058$	$0.826 \pm 0.035$	$0.292 \pm 0.012$	$-0.074 \pm 0.027$	$0.397 \pm 0.023$	$0.127 \pm 0.006$
Random	1420	$0.458 \pm 0.028$	$0.032 \pm 0.073$	$0.923 \pm 0.056$	$0.346 \pm 0.065$	$-0.060 \pm 0.033$	$0.428 \pm 0.044$	$0.157 \pm 0.010$
Multivariate	1420	$0.737 \pm 0.004$	$0.156 \pm 0.033$	$0.635 \pm 0.011$	$0.213 \pm 0.011$	$0.031 \pm 0.016$	$0.248 \pm 0.014$	$0.095 \pm 0.006$
kNN								
$k = 3$	1420	$0.699 \pm 0.017$	$0.174 \pm 0.059$	$0.674 \pm 0.015$	$0.232 \pm 0.017$	$0.034 \pm 0.029$	$0.256 \pm 0.014$	$0.150 \pm 0.008$
$k = 10$	1420	$0.715 \pm 0.014$	$0.189 \pm 0.040$	$0.652 \pm 0.013$	$0.214 \pm 0.009$	$0.040 \pm 0.019$	$0.240 \pm 0.010$	$0.099 \pm 0.004$
$k = 20$	1420	$0.686 \pm 0.030$	$0.199 \pm 0.061$	$0.679 \pm 0.030$	$0.227 \pm 0.014$	$0.041 \pm 0.010$	$0.248 \pm 0.013$	$0.105 \pm 0.008$


**Figure 7.** The  $W2$  magnitude versus redshift for the SDSS sample. The binning of the 96 181 sources is for equal  $z_{\text{spec}}$  spacing, with the error bars on the abscissa showing the range and the error bars on the ordinate  $\pm 1\sigma$ .

We note that in all three cases, the normalised median absolute deviation (the metric chosen by Carvajal et al. 2021) appears to be the clearest tracer of the degradation of the performance as more missing magnitudes are imputed. As discussed in Sect. 2.2.1, and illustrated in Fig. 3, however, around half of the OCARS sources have no SDSS magnitudes due to their location in the sky. Since the SKA and its pathfinders are restricted to surveying the southern sky, we can expect very little overlap with the SDSS, thus not having all of the magnitudes required to predict redshifts. However, *SkyMapper* (Wolf et al. 2018)<sup>7</sup>, which is currently surveying the southern sky, uses similar bands to the SDSS ( $u, v, g, r, i, z$ ) and so we expect a model trained upon SDSS data to still be applicable. Of course, once the *SkyMapper* catalogue becomes sufficiently large, the photometry from these sources can also be used to build a model.

In order to demonstrate the performance of the test data with up to two missing magnitudes, from the original un-imputed data we retain only those with less than three missing values before performing multivariate imputation. These are then trained using the


**Figure 8.** The spread in  $\Delta z$  as more  $z$  missing magnitudes are imputed for each source using the multivariate method. From a single Deep Learning run so the standard deviations are approximate.

<sup>7</sup> <https://skymapper.anu.edu.au>

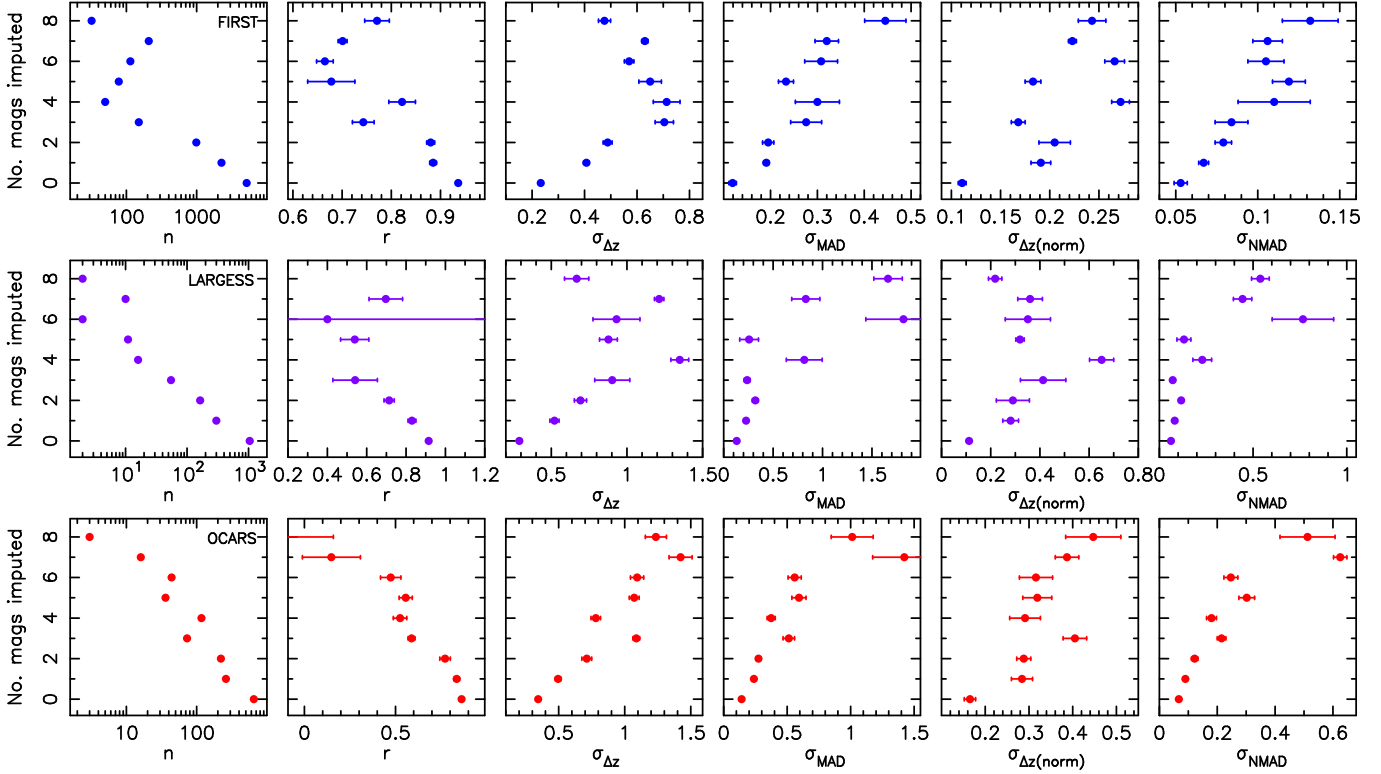


**Figure 9.** The performance of the Deep Learning for different numbers of imputed magnitudes per source for the FIRST (top) & LARGESS (middle) QSOs and OCARS quasars with at least one SDSS magnitude (bottom). The error bars show the  $\pm 1\sigma$  from the mean of 10 trials.

same model, created by the non-imputed SDSS data, on all three sets. We show the results in Fig. 10, from which we see:

- (i) FIRST:  $r \approx 0.93$  and  $\sigma_{\text{NMAD}} \approx 0.055$ , while retaining 93% of the data, compared to  $\bar{r} = 0.95$  and  $\overline{\sigma_{\text{NMAD}}} = 0.052$  for the 57% remaining when the sources with any missing values are excluded.
- (ii) LARGESS:  $r \approx 0.87$  and  $\sigma_{\text{NMAD}} \approx 0.063$  for 94% of the sample, compared to  $\bar{r} = 0.91$  and  $\overline{\sigma_{\text{NMAD}}} = 0.061$  for 65%.
- (iii) OCARS, with at least one SDSS magnitude,  $r \approx 0.84$  and  $\sigma_{\text{NMAD}} \approx 0.068$  for 80%, compared to  $\bar{r} = 0.87$  and  $\overline{\sigma_{\text{NMAD}}} = 0.066$  for 46%.

The NMAD values are within the range of those in the literature,  $\sigma_{\text{NMAD}} = 0.029$  (Laurino et al. 2011),  $0.012 - 0.058$  (Brescia et al. 2013),  $0.060 - 0.065$  (Ananna et al. 2017),  $0.014 - 0.401$  (Duncan et al. 2018),  $0.026$  (D’Isanto & Polsterer 2018),  $> 0.016$  (Beck et al. 2021),  $0.091$  (Carvajal et al. 2021) and  $> 0.079$  (Li et al. 2021). Unlike these, however, our predictions are from an optically selected training model applied to radio selected samples. Moreover, these include sources with up to two missing magnitudes each.

#### 4 CONCLUSIONS

The requirement of all nine *FUV*, *NUV*, *u*, *g*, *r*, *i*, *z*, *W1*, *W2* bands to optimally predict photometric redshifts using machine learning techniques can cause a significant reduction in the number of sources to which the model is applicable. We therefore explore various methods of imputation to replace the missing data, comparing the results with those of the non-imputed data. For the SDSS training data, 28% of the sources have incomplete photometry and we find simple imputation to be effective, particularly replacing the

missing magnitude with the maximum value for that band. This method is similar to that of Carvajal et al. (2021), who assume that missing data are at the detection limit. All of the tested methods perform well, however, giving a regression coefficient of the least-squares linear fit between the predicted and measured redshifts of  $r > 0.9$  and a normalised median absolute deviation, which is found to be the best metric to quantify the effect of imputation, of  $\sigma_{\text{NMAD}} < 0.06$ .

Our aim is to use the Deep Learning to train models for radio-selected sources, similar to those expected to be detected with the SKA and its pathfinders. For our three test datasets the number of sources with missing magnitudes ranges from 35% to 79%, which would clearly benefit from effective imputation. Testing these, we find simple imputation to produce inferior models to multivariate imputation, which uses machine learning to replace the missing values based upon the features in the data. We suggest that this is since a large fraction of the missing SDSS data will indeed be due to sensitivity limits (in particular the *u*, *g*, *r*, *i*, *z* magnitudes), whereas for the other datasets these may just not have been observed. This will certainly be the case for the OCARS sources, of which only about half overlap the same region of sky surveyed by the SDSS with only half again having all of the magnitudes. This will also be an issue for the SKA and its pathfinders, although using SkyMapper, which will observe similar optical bands as the SDSS over the southern sky, to obtain the photometry will address this.

Testing various levels of imputation, we note a steep decrease in performance when more than two missing magnitudes are replaced, for all of the test datasets. Also, the fraction of sources with more than two missing values is small. We therefore suggest limiting the imputation to this number per source and, applying this, we find the performance to be similar to that of the non-imputed data,

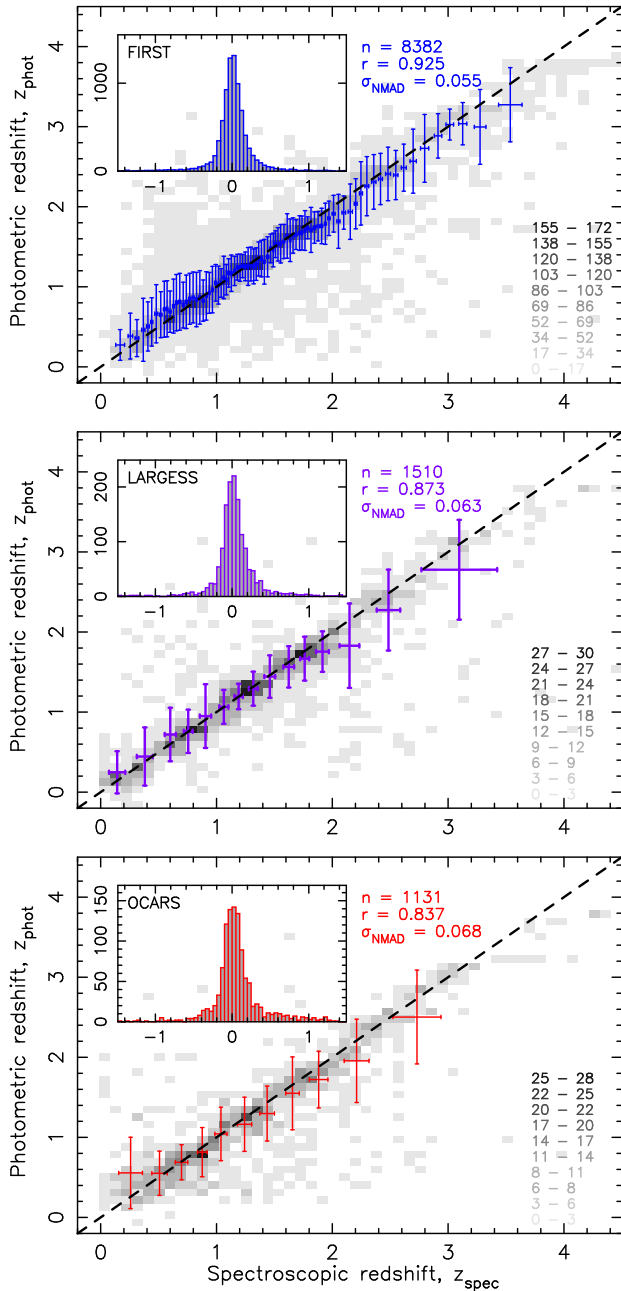


**Figure 10.** The results a single Deep Learning run on the test data sets missing up to two magnitudes per source. The binning is for an equal number of sources in each bin (100) with the error bars showing  $\pm 1\sigma$ . The broken line shows  $z_{\text{phot}} = z_{\text{spec}}$  and the inset the distribution of  $\Delta z$ .

although with significant increases in sample sizes. We also find the results to be comparable to those in the literature, which all, but one, use only complete data and all of which are tested upon the same dataset used to train the model.

Of the three training sets, two (FIRST & LARGESS) do have a large overlap with the SDSS and, with mean radio flux densities of  $S_{\text{radio}} \sim 20$  mJy (Curran et al. 2021), these may be representative of the radio continuum sources which will be detected with the SKA pathfinders (e.g. Norris et al. 2011). The other training set, OCARS, forms a VLBI calibration catalogue and so has much higher fluxes ( $S_{\text{radio}} = 340$  mJy). Furthermore, OCARS only overlaps with the SDSS over one half of the sky. However, if

we select OCARS sources with at least one SDSS magnitude, imputing up to two missing values returns 80% of the sample while yielding an NMAD comparable to those discussed above. The fact that application of the Deep Learning method on imputed data from disparate databases gives similarly good results makes us confident in the applicability of such techniques to radio sources detected with the SKA and its pathfinders.

## ACKNOWLEDGEMENTS

I wish to thank the referee for their prompt and helpful comments. This research has made use of the NASA/IPAC Extragalactic Database (NED) which is operated by the Jet Propulsion Laboratory, California Institute of Technology, under contract with the National Aeronautics and Space Administration and NASA’s Astrophysics Data System Bibliographic Service. This research has also made use of NASA’s Astrophysics Data System Bibliographic Service.

## DATA AVAILABILITY

Data and SDSS TensorFlow training model available on request.

## REFERENCES

- Alam S. et al., 2015, *ApJS*, 219, 12  
 Ananna T. T. et al., 2017, *ApJ*, 850, 66  
 Beck R., Dobos L., Budavári T., Szalay A. S., Csabai I., 2017, *Astronomy and Computing*, 19, 34  
 Beck R., Szapudi I., Flewelling H., Holmberg C., Magnier E., 2021, *MNRAS*, 500, 1633  
 Becker R. H., White R. L., Helfand D. J., 1995, *ApJ*, 450, 559  
 Bianchi L., Shiao B., Thilker D., 2017, *ApJS*, 230, 24  
 Bovy J. et al., 2012, *ApJ*, 749, 41  
 Brescia M., Cavuoti S., D’Abrusco R., Longo G., Mercurio A., 2013, *ApJ*, 772, 140  
 Carvajal R., Matute I., Afonso J., Amarantidis S., Barbosa D., Cunha P., Humphrey A., 2021, A New Window on the Radio Emission from Galaxies, Galaxy Clusters and Cosmic Web: Current Status and Perspectives  
 Ching J. H. Y. et al., 2017, *MNRAS*, 464, 1306  
 Curran S. J., 2020, *MNRAS*, 493, L70  
 Curran S. J., Moss J. P., 2019, *A&A*, 629, A56  
 Curran S. J., Moss J. P., Perrott Y. C., 2021, *MNRAS*, 503, 2639  
 D’Isanto A., Polsterer K. L., 2018, *A&A*, 609, 111  
 Duncan K. J. et al., 2018, *MNRAS*, 473, 2655  
 Glowacki M., Allison J. R., Sadler E. M., Moss V. A., Jarrett T. H., 2017, *MNRAS*, submitted (arXiv:1709.08634)  
 Han B., Ding H.-P., Zhang Y.-X., Zhao Y.-H., 2016, *Research in Astronomy and Astrophysics*, 16, 74  
 Hildebrandt H. et al., 2010, *A&A*, 523, A31  
 Laurino O., D’Abrusco R., Longo G., Riccio G., 2011, *MNRAS*, 418, 2165  
 Li C. et al., 2021, *MNRAS*, 509, 2289  
 Little R. J. A., Rubin D. B., 1986, *Statistical Analysis with Missing Data*. John Wiley & Sons, New York  
 Luken K. J., Norris R. P., Park L. A. F., 2019, *PASP*, 131, 108003  
 Ma C. et al., 2009, *IERS Technical Note*, 35, 1  
 Maddox N., Hewett P. C., Péroux C., Nestor D. B., Wisotzki L., 2012, *MNRAS*, 424, 2876

- Malkin Z., 2018, *ApJS*, 239, 20  
Norris R. P. et al., 2011, *PASA*, 28, 215  
Pâris I. et al., 2018, *A&A*, 613, A51  
Richards G. T. et al., 2001, *AJ*, 122, 1151  
Salvato M., Ilbert O., Hoyle B., 2019, *Nature Astronomy*, 3, 212  
Skrutskie M. F. et al., 2006, *AJ*, 131, 1163  
Troyanskaya O., Cantor M., Sherlock G., Brown P., Hastie T., Tibshirani R., Botstein D., Altman R. B., 2001, *Bioinformatics*, 17, 520  
van Buuren S., Groothuis-Oudshoorn K., 2011, *Journal of Statistical Software*, 45, 1  
Weinstein M. A. et al., 2004, *ApJS*, 155, 243  
White R. L., Becker R. H., Helfand D. J., Gregg M. D., 1997, *ApJ*, 475, 479  
Wolf C. et al., 2018, *PASA*, 35, 10  
Wright E. L. et al., 2010, *AJ*, 140, 1868